

**EFFECT OF LANTHANUM OXIDE (La_2O_3)
ADDITION ON THE PROPERTIES OF CALCIUM
COPPER TITANATE ($\text{CaCu}_3\text{Ti}_4\text{O}_{12}$)**

NUR SHAFIZA AFZAN BINTI SHARIF

UNIVERSITI SAINS MALAYSIA

2010

**EFFECT OF LANTHANUM OXIDE (La_2O_3) ADDITION ON THE
PROPERTIES OF CALCIUM COPPER TITANATE ($\text{CaCu}_3\text{Ti}_4\text{O}_{12}$)**

by

NUR SHAFIZA AFZAN BINTI SHARIF

**Thesis submitted in fulfillment of the requirements
for the degree of
Master of Science**

December 2010

DECLARATION

I hereby declare that I have conducted, completed the research work and written the dissertation entitles “Effect of Lanthanum Oxide (La_2O_3) Addition on the Properties of Calcium Copper Titanate ($\text{CaCu}_3\text{Ti}_4\text{O}_{12}$)”. I also declare that it has not been previously submitted for the award of any degree or diploma or other similar title of this for any other examining body or University.

Candidate’s Name : Nur Shafiza Afzan Bt Sharif

Signature :

Date :

Supervisor’s Name : Assoc. Prof. Dr. Sabar Derita Hutagalung

Signature :

Date :

Co-supervisor’s Name: Prof. Dr. Haji Zainal Arifin Ahmad

Signature :

Date :

ACKNOWLEDGEMENT

Firstly, I would like to express my sincere appreciation to those who contributed in this thesis, without their help it would not been success. It is very hard to completely writing a thesis without co-operation and help from many peoples. Frankly, conducive and privileged research environment which has been provided by the School of Materials and Mineral Resources Engineering, Universiti Sains Malaysia is very helpful for me in order to realize my capability and show me my strength and weakness as well.

This appreciation is also dedicated to my high spirited supervisor, Assoc. Prof. Dr. Sabar Derita Hutagalung in the first place or his major contributions to the successful of this project, as well as my co-supervisor, Prof. Dr. Haji Zainal Arifin Ahmad for providing the knowledge base for my future. Moreover, I like to thanks Prof. Dr. Mohamad Deraman, Universiti Kebangsaan Malaysia (External Examiner), and Dr. Julie Juliewatty Mohamed, Universiti Sains Malaysia (Internal Examiner) for their valuable comments and suggestions.

Appreciations also go to all the staffs, especially Mr. Shahrul Ami Zainal Abidin, Madam Fong Lee Lee, Mr. Farid Abd. Rahim, Mr. Shahid Abd. Jalal, Mr. Abdul Rashid Selamat, Mr. Suhaimi Sulong and Mrs. Haslina Zulkifli for their technical support, as well as my postgraduate members, Azwadi Sulaiman, Aliyah Jamaludin, Che Engku Suhaimi Che Engku Ali and many more for the instruction and the moral support. I appreciate all the wonderful and precious moments with the team that we shared together. Special thanks to my family for their love and continued support. Lastly, I would like to extend my appreciation to all of my friends and to all those people who were directly or indirectly involved in this project.

TABLE OF CONTENTS

ACKNOWLEDGEMENTS	ii
TABLE OF CONTENTS	iii
LIST OF TABLES	viii
LIST OF FIGURES	x
LIST OF APPENDICES	xvii
LIST OF ABBREVIATION	xx
LIST OF MAIN SYMBOL	xxi
ABSTRAK	xxiii
ABSTRACT	xxv
CHAPTER 1: INTRODUCTION	
1.1 Ceramic Materials	1
1.2 Preparation of $\text{CaCu}_3\text{Ti}_4\text{O}_{12}$ (CCTO)	3
1.3 Problem Statement	4
1.4 Research Objectives	6
1.5 Research Overview	6
CHAPTER 2: LITERATURE REVIEW	
2.1 Introduction	9
2.2 Perovskite Structure	9
2.3 CCTO	11
2.4 Dielectric Materials	13
2.4.1 Dielectric Properties	13

2.4.2	Polarization Mechanisms	16
2.4.3	Impedance Spectroscopy	17
2.4.3.1	Impedance Spectroscopy of CCTO	18
2.5	Grain Boundaries Effect	23
2.6	Processing Effect	25
2.7	Electrode/Sample Contact Effect	26
2.8	Properties Modification for CCTO Ceramics	28
2.8.1	Doping Effect and Substitution Mechanisms	28
2.8.2	Acceptor Dopant	30
2.8.3	Donor Dopant	31
2.9	Microwave Heating	32
2.9.1	Susceptor	35
2.9.1.1	Silicon Carbide Susceptor	35
2.9.1.2	Graphite Susceptor	36
2.9.2	Effect of Microwave Heating	36

CHAPTER 3: MATERIALS AND METHODOLOGY

3.1	Introduction	39
3.2	Starting Materials	41
3.3	Processing Steps	41
3.3.1	Composition Formulation	41
3.3.2	Mixing Process	42
3.3.3	Calcination	43
3.3.4	De-agglomeration	45
3.3.5	Uniaxial Pressing	45

3.3.6	Sintering	47
3.3.7	Heat Treatment Using Microwave Oven	49
3.3.8	Sample Contact/Electrode	50
3.4	Sample Preparation and Characterization Technique	50
3.4.1	X-ray Diffraction (XRD)	51
3.4.2	Scanning Electron Microscope (SEM)	52
3.4.3	Density Test	56
3.4.4	Dielectric Properties Measurement	56

CHAPTER 4: RESULTS AND DISCUSSION

4.1	Introduction	60
4.2	Characterization of Starting Materials	60
4.2.1	Calcium Hydroxide (Ca(OH) ₂) Powder	60
4.2.2	Copper Oxide (CuO) Powder	62
4.2.3	Titanium Oxide (TiO ₂) Powder	63
4.2.4	Lanthanum oxide (La ₂ O ₃) Powder	64
4.3	Synthesis of CCTO	65
4.3.1	Microstructure of sintered CCTO Ceramics	69
4.3.2	Dielectric Behavior of CCTO	71
4.3.2.1	Cole-Cole Plot	77
4.4	Preparation of La-doped CCTO	79
4.4.1	Phase Evolution of Ca _{1-x} La _x Cu ₃ Ti ₄ O ₁₂ Ceramics	79
4.4.2	Microstructure of Sintered Ca _{1-x} La _x Cu ₃ Ti ₄ O ₁₂ Ceramics	86
4.4.2.1	Surface Microstructure for Samples Synthesized without Argon Gas	86

4.4.2.2 Fracture Surface for Samples Synthesized without Argon Gas	88
4.4.2.3 Density Measurement	90
4.4.2.4 Surface Microstructure for Samples Synthesized under Argon Environment	91
4.4.2.5 Fracture Surface for Samples Synthesized under Argon Environment	95
4.4.2.6 Density of $\text{Ca}_{1-x}\text{La}_x\text{Cu}_3\text{Ti}_4\text{O}_{12}$ Ceramics	97
4.4.3 Dielectric Behavior of $\text{Ca}_{1-x}\text{La}_x\text{Cu}_3\text{Ti}_4\text{O}_{12}$	98
4.4.3.1 Dielectric Behaviour of CCTO Samples Synthesized without gas	98
4.4.3.2 Dielectric Behavior of $\text{Ca}_{1-x}\text{La}_x\text{Cu}_3\text{Ti}_4\text{O}_{12}$ at 1 MHz	100
4.4.3.3 Cole-Cole Plot for CCTO Samples with Various La Concentration	101
4.4.3.4 Dielectric Behavior for Samples Synthesized Under Argon Environment	105
4.4.3.5 Dielectric Behavior of $\text{Ca}_{1-x}\text{La}_x\text{Cu}_3\text{Ti}_4\text{O}_{12}$ at 1 MHz	111
4.4.3.6 Impedance Spectroscopy Study for Samples Synthesized under Argon Environment	112
4.4.3.7 Dielectric Behavior using Different Electrode Synthesized under Argon Environment	115
4.4.3.8 Impedance Characteristic of $\text{Ca}_{1-x}\text{La}_x\text{Cu}_3\text{Ti}_4\text{O}_{12}$ Ceramics	119

4.5	Heat Treatment using Microwave Processing	121
4.5.1	Microstructure of Post heated Sample using SiC Susceptor	123
4.5.2	Dielectric Behavior of Post heated Sample using Microwave Oven	124
CHAPTER 5 : CONCLUSION AND RECOMMENDATION		
5.1	Conclusion	127
5.2	Recommendation for Future Research	128
REFERENCES		130
APPENDICES		140
LIST OF PUBLICATIONS AND CONFERENCES		167

LIST OF TABLES

Table 2.1	The value of dielectric constant for some materials at room temperatures	15
Table 3.1	Weight of raw materials to prepare 30 g batch powder of undoped and La-doped CCTO	42
Table 4.1	Lattice parameter and crystallite size of $\text{Ca}_{1-x}\text{La}_x\text{Cu}_3\text{Ti}_4\text{O}_{12}$ with various concentration of x according to peak (220)	83
Table 4.2	Mean grain size and standard deviation of $\text{Ca}_{1-x}\text{La}_x\text{Cu}_3\text{Ti}_4\text{O}_{12}$ samples sintered without gas	88
Table 4.3	Mean grain size and standard deviation of $\text{Ca}_{1-x}\text{La}_x\text{Cu}_3\text{Ti}_4\text{O}_{12}$ samples sintered with gas	94
Table 4.4	Resistance values due to grain and grain boundary, bulk resistance and resistivity of $\text{Ca}_{1-x}\text{La}_x\text{Cu}_3\text{Ti}_4\text{O}_{12}$ samples with various mole concentration of La	104
Table 4.5	Domain and grain resistance for $\text{Ca}_{1-x}\text{La}_x\text{Cu}_3\text{Ti}_4\text{O}_{12}$ samples with various mole concentration of La measured at high frequency	105
Table 4.6	Comparison of dielectric constant synthesized without argon and under argon environment at same temperature, duration and using same sample contact at frequency 1 MHz	106
Table 4.7	Resistance values due to grain and grain boundary, bulk resistance and resistivity of $\text{Ca}_{1-x}\text{La}_x\text{Cu}_3\text{Ti}_4\text{O}_{12}$ samples with various mole concentration of La	114

Table 4.8	Resistance values due to domain and grain of $\text{Ca}_{1-x}\text{La}_x\text{Cu}_3\text{Ti}_4\text{O}_{12}$ samples with various mole concentration of La	115
Table 4.9	Resistance values due to grain and grain boundary, bulk resistance and resistivity of $\text{Ca}_{1-x}\text{La}_x\text{Cu}_3\text{Ti}_4\text{O}_{12}$ samples with various mole concentration of La	120
Table 4.10	Resistance values due to domain and grain of $\text{Ca}_{1-x}\text{La}_x\text{Cu}_3\text{Ti}_4\text{O}_{12}$ samples with various mole concentration of La	121

LIST OF FIGURES

Figure 1.1	Process flow of experimental work	8
Figure 2.1	Perovskite simple cubic structures	10
Figure 2.2	Crystal structure of CCTO	11
Figure 2.3	A parallel-plate capacitor (a) when a vacuum is present and (b) when a dielectric material is present	15
Figure 2.4	Schematic representations of different mechanisms of polarization	17
Figure 2.5	An equivalent circuit for electroceramic	19
Figure 2.6	The RC equivalent circuit model, R_g , C_g ; R_{gb} , C_{gb} ; and R_e , C_e are the resistance and capacitances associated with grain, grain boundaries and the electrodes	20
Figure 2.7	Equivalent circuit of electrode effect on ceramic material	22
Figure 2.8	Limiting grain size for ferroelectric domain formation	23
Figure 2.9	Comparison of the time–temperature profiles for microwave and conventional synthesis of BMT	33
Figure 2.10	Schematic representations of a domestic microwave oven and an external temperature controller	34
Figure 2.11	Microwave heating of graphite	36
Figure 3.1	(a) Plastic bottle for wet mixing process, and (b) Cylindrical zirconia ball as media	43
Figure 3.2	Temperature profile for calcination of undoped and La-doped CCTO powder	44

Figure 3.3	Alumina crucible used to calcine undoped and La-doped CCTO powder: (a) cup shape and (b) boat shape	45
Figure 3.4	A die mold set for uniaxial pressing	46
Figure 3.5	For a powder compact, micro-structural changes occur during firing, (a) powder particles after pressing, (b) particle coalescence and pore formation as sintering begins and (c) as sintering proceeds, the pores change size and shape	48
Figure 3.6	Temperature profile for sintering of undoped and La-doped CCTO pellet	48
Figure 3.7	Temperature profile for sintering of $\text{Ca}_{1-x}\text{La}_x\text{Cu}_3\text{Ti}_4\text{O}_{12}$ under argon environment at cooling stage	49
Figure 3.8	Susceptor for microwave heating made from 40 wt. % coarse silicon carbide particles distributed in an alumina cement matrix	50
Figure 3.9	Schematic diagram of an X-ray diffractometer; T = X-ray source, S = specimen, C = detector and O = the axis around which the specimen and detector rotate	52
Figure 3.10	Schematic of Scanning Electron Microscope (SEM)	54
Figure 3.11	(a) Required equipment for dielectric material measurement (b) Basic flow for dielectric material measurements at high frequency	57 58
Figure 3.12	Basic flows for dielectric material measurements at low frequency	59
Figure 4.1	SEM micrograph of $\text{Ca}(\text{OH})_2$ powder	61
Figure 4.2	XRD pattern of $\text{Ca}(\text{OH})_2$ powder	61

Figure 4.3	SEM Micrograph of CuO powder	62
Figure 4.4	XRD pattern of CuO powder	63
Figure 4.5	SEM Micrograph of TiO ₂ powder	63
Figure 4.6	XRD pattern of TiO ₂ powder	64
Figure 4.7	SEM micrograph of La ₂ O ₃ powder	65
Figure 4.8	XRD pattern of La ₂ O ₃ powder	65
Figure 4.9	Mixture powder of Ca(OH) ₂ -CuO-TiO ₂	66
Figure 4.10	CCTO powder after calcinations process	66
Figure 4.11	XRD pattern of CCTO powders calcined at 900 °C for 12 hours	67
Figure 4.12	(a) Calcined and (b) sintered CCTO pellets	68
Figure 4.13	X-ray diffraction pattern of sintered CCTO (a) without argon gas and (b) under argon environment	69
Figure 4.14	SEM images of surface and fracture surface: (a) and (b) sintered without gas, (c) and (d) sintered with gas, respectively	70
Figure 4.15	Dielectric constant at high frequency for undoped CCTO sintered at 1000 °C for 10 hours without argon gas. Inset is close up of dielectric constant value from 1 MHz to 20 MHz	72
Figure 4.16	Plots of dielectric loss at high frequency for CCTO sintered without argon gas using Al electrode	73
Figure 4.17	Dielectric constant of undoped CCTO sintered with and without gas using Al electrode	74
Figure 4.18	Plot of dielectric constant versus log frequency for CCTO sintered with argon gas using Al and Ag electrodes	76
Figure 4.19	The dielectric loss as a function of frequency of undoped CCTO sample sintered under argon gas using different electrode	77

Figure 4.20	Cole-Cole plot for CCTO ceramic sample sintered without argon gas at low frequency	78
Figure 4.21	XRD results for $\text{Ca}_{1-x}\text{La}_x\text{Cu}_3\text{Ti}_4\text{O}_{12}$ ceramics with various concentration of La calcined at 900 °C for 12 hours	80
Figure 4.22	XRD patterns of $\text{Ca}_{1-x}\text{La}_x\text{Cu}_3\text{Ti}_4\text{O}_{12}$ with various concentration of La sintered ceramics without argon gas at cooling stage	81
Figure 4.23	Close-up of X-ray diffraction patterns of $\text{Ca}_{1-x}\text{La}_x\text{Cu}_3\text{Ti}_4\text{O}_{12}$ sintered pellets with different mol percentage (x)	83
Figure 4.24	Variation in lattice parameter and crystallite size with different La doping concentration	83
Figure 4.25	XRD patterns of $\text{Ca}_{1-x}\text{La}_x\text{Cu}_3\text{Ti}_4\text{O}_{12}$ with various La concentrations, sintered under argon environment at cooling stage	85
Figure 4.26	Variation in lattice parameter with different La doping concentration for samples sintered with gas	85
Figure 4.27	SEM micrographs of $\text{Ca}_{1-x}\text{La}_x\text{Cu}_3\text{Ti}_4\text{O}_{12}$ samples sintered using Carbolite Furnace	87
Figure 4.28	Grain size distribution of $\text{Ca}_{1-x}\text{La}_x\text{Cu}_3\text{Ti}_4\text{O}_{12}$ sintered pellets without gas	88
Figure 4.29	Microstructure of fracture surface of 0, 2, 5 and 10 mole % La sintered without argon gas	89
Figure 4.30	EDX analysis of fracture surface for sample with x = 0.05 La	89
Figure 4.31	Density and porosity of sintered pellets prepared from electrical furnace technique	91

Figure 4.32	SEM micrographs of sintered $\text{Ca}_{1-x}\text{La}_x\text{Cu}_3\text{Ti}_4\text{O}_{12}$ samples using High Temperature Tube Furnace	93
Figure 4.33	Grain size distributions of $\text{Ca}_{1-x}\text{La}_x\text{Cu}_3\text{Ti}_4\text{O}_{12}$ samples synthesized under argon environment	94
Figure 4.34	Fracture surface of sintered $\text{Ca}_{1-x}\text{La}_x\text{Cu}_3\text{Ti}_4\text{O}_{12}$ samples prepared via High Temperature Tube Furnace	96
Figure 4.35	EDX analysis of surface morphology for La-doped CCTO with 3 mole % La	96
Figure 4.36	Density of $\text{Ca}_{1-x}\text{La}_x\text{Cu}_3\text{Ti}_4\text{O}_{12}$ samples synthesis under argon environment	97
Figure 4.37	Frequency dependence of the dielectric constant for $\text{Ca}_{1-x}\text{La}_x\text{Cu}_3\text{Ti}_4\text{O}_{12}$ pellets synthesized without argon gas and evaporated with Al electrode. Inset is close up of dielectric constant at frequency 10 – 1000 MHz	99
Figure 4.38	Dielectric loss ($\tan \delta$) of $\text{Ca}_{1-x}\text{La}_x\text{Cu}_3\text{Ti}_4\text{O}_{12}$ sintered without argon gas at cooling stage. Inset is close up of dielectric loss at frequency 10 – 1000 MHz	100
Figure 4.39	Dielectric constant and dielectric loss of $\text{Ca}_{1-x}\text{La}_x\text{Cu}_3\text{Ti}_4\text{O}_{12}$ ceramics at frequency 1 MHz	101
Figure 4.40	Cole-Cole plot measured at low frequency (1 Hz – 1 MHz) for $\text{Ca}_{1-x}\text{La}_x\text{Cu}_3\text{Ti}_4\text{O}_{12}$ samples using Al electrode	104
Figure 4.41	Cole-Cole plot measured at high frequency (1 MHz – 1 GHz) for $\text{Ca}_{1-x}\text{La}_x\text{Cu}_3\text{Ti}_4\text{O}_{12}$ samples using Al electrode	105

Figure 4.42	Dielectric constant of $\text{Ca}_{1-x}\text{La}_x\text{Cu}_3\text{Ti}_4\text{O}_{12}$ sintered under argon environment at cooling stage and evaporated with Al electrode. Inset is close up of dielectric constant at frequency 10 – 1000 MHz	106
Figure 4.43	Dissipation factor ($\tan \delta$) of $\text{Ca}_{1-x}\text{La}_x\text{Cu}_3\text{Ti}_4\text{O}_{12}$ sintered under argon environment at cooling stage and evaporated with Al electrode. Inset is close up of dielectric loss at frequency 10 – 1000 MHz	110
Figure 4.44	Dielectric constant and dielectric loss of La-doped CCTO ceramics at frequency 1 MHz using Al electrodes	111
Figure 4.45	Impedance plots at low frequency for $\text{Ca}_{1-x}\text{La}_x\text{Cu}_3\text{Ti}_4\text{O}_{12}$ synthesized under argon environment using Al electrode	114
Figure 4.46	Impedance plots at high frequency for $\text{Ca}_{1-x}\text{La}_x\text{Cu}_3\text{Ti}_4\text{O}_{12}$ synthesized under argon environment using Al electrode	115
Figure 4.47	Dielectric constant of $\text{Ca}_{1-x}\text{La}_x\text{Cu}_3\text{Ti}_4\text{O}_{12}$ sintered under argon environment at cooling stage and evaporated with Ag electrode	117
Figure 4.48	Comparison of dielectric constant value using Ag and Al electrode for ceramic $\text{Ca}_{1-x}\text{La}_x\text{Cu}_3\text{Ti}_4\text{O}_{12}$ at frequency 1 MHz	117
Figure 4.49	Dissipation factor ($\tan \delta$) of $\text{Ca}_{1-x}\text{La}_x\text{Cu}_3\text{Ti}_4\text{O}_{12}$ sintered under argon environment at cooling stage and evaporated with Ag electrode	119
Figure 4.50	Impedance spectroscopy plot of $\text{Ca}_{1-x}\text{La}_x\text{Cu}_3\text{Ti}_4\text{O}_{12}$ ceramic sample at low frequency using Ag electrode	120

Figure 4.51	Impedance spectroscopy plot of $\text{Ca}_{1-x}\text{La}_x\text{Cu}_3\text{Ti}_4\text{O}_{12}$ ceramic sample at high frequency using Ag electrode	121
Figure 4.52	SiC crucible position	122
Figure 4.53	SEM of surface for microwave post heated 3 mole % La pellets: (a) 30 min and (b) 60 min	123
Figure 4.54	SEM of fractures surface for microwave post heated 3 mole % La pellets: (a) 30 min and (b) 60 min	124
Figure 4.55	Frequency dependence of room temperature (a) dielectric constant and (b) dielectric loss of sintered sample at 1000 °C for 10 hours without and with microwave treatment for 30 and 60 minutes	126

LIST OF APPENDICES

APPENDIX A	Weight of Starting Materials	140
APPENDIX B	Calculation on Starting Materials Needed to Prepare a Batch of 30 g $\text{CaCu}_3\text{Ti}_4\text{O}_{12}$	141
APPENDIX C	Calculation on Starting Materials Needed to Prepare a Batch of 30 g $\text{Ca}_{0.99}\text{La}_{0.01}\text{Cu}_3\text{Ti}_4\text{O}_{12}$	142
APPENDIX D	Calculation on Starting Materials Needed to Prepare a Batch of 30 g $\text{Ca}_{0.98}\text{La}_{0.02}\text{Cu}_3\text{Ti}_4\text{O}_{12}$	143
APPENDIX E	Calculation on Starting Materials Needed to Prepare a Batch of 30 g $\text{Ca}_{0.97}\text{La}_{0.03}\text{Cu}_3\text{Ti}_4\text{O}_{12}$	144
APPENDIX F	Calculation on Starting Materials Needed to Prepare a Batch of 30 gram $\text{Ca}_{0.95}\text{La}_{0.05}\text{Cu}_3\text{Ti}_4\text{O}_{12}$	145
APPENDIX G	Calculation on Starting Materials Needed to Prepare a Batch of 30 g $\text{Ca}_{0.90}\text{La}_{0.10}\text{Cu}_3\text{Ti}_4\text{O}_{12}$	146
APPENDIX H	Powder Diffraction File of $\text{Ca}(\text{OH})_2$	147
APPENDIX I	Powder Diffraction File of CuO	148
APPENDIX J	Powder Diffraction File of TiO_2	149
APPENDIX K	Powder Diffraction File of La_2O_3	150
APPENDIX L	Powder Diffraction File of $\text{CaCu}_3\text{Ti}_4\text{O}_{12}$	151
APPENDIX M	Calculation on Lattice Parameter of $\text{Ca}_{1-x}\text{La}_x\text{Cu}_3\text{Ti}_4\text{O}_{12}$ Samples	152
APPENDIX N	Calculation on Crystallite Size of $\text{Ca}_{1-x}\text{La}_x\text{Cu}_3\text{Ti}_4\text{O}_{12}$ Samples	153

APPENDIX O	Complex Impedance Measurement	
	i. Complex impedance plane plots for	154
	Ca _{1-x} La _x Cu ₃ Ti ₄ O ₁₂ synthesized without argon gas	
	using Al electrode measured at low frequency	
	ii. Complex impedance plane plots for	155
	Ca _{1-x} La _x Cu ₃ Ti ₄ O ₁₂ synthesized without argon gas	
	using Al electrode measured at high frequency	
APPENDIX P	Cole-Cole Plot Measurement	
	i. Impedance plots at low frequency for	156
	Ca _{1-x} La _x Cu ₃ Ti ₄ O ₁₂ synthesized under argon	
	environment using Al electrode measured at low	
	frequency	
	ii. Impedance plots at low frequency for	157
	Ca _{1-x} La _x Cu ₃ Ti ₄ O ₁₂ synthesized under argon	
	environment using Al electrode measured at high	
	frequency	
APPENDIX Q	Cole-Cole Plot Measurement	
	i. Impedance plots at low frequency for	158
	Ca _{1-x} La _x Cu ₃ Ti ₄ O ₁₂ synthesized under argon	
	environment using Ag electrode measured at low	
	frequency	
	ii. Impedance plots at low frequency for	159
	Ca _{1-x} La _x Cu ₃ Ti ₄ O ₁₂ synthesized under argon	
	environment using Ag electrode measured at high	
	frequency.	

APPENDIX R	Calculation of Resistivity in Complex Impedance Plot at Low Frequency	160
APPENDIX S	Grain Size Distribution	162

LIST OF ABBREVIATIONS

$\text{CaCu}_3\text{Ti}_4\text{O}_{12}$ (CCTO)	Calcium Copper Titanate
$\text{Ca}_{1-x}\text{La}_x\text{Cu}_3\text{Ti}_4\text{O}_{12}$	La-doped $\text{CaCu}_3\text{Ti}_4\text{O}_{12}$ with x mole fraction of La
SEM	Scanning electron microscopy
XRD	X-ray diffraction
EDX	Energy-dispersive X-ray spectroscopy
VPFESEM	Variable pressure field emission SEM

LIST OF MAIN SYMBOLS

%	Percentage
°	Degree
°C	Degree Celsius
°C/min	Degree Celsius per minutes
J	Joule
MPa	Mega Pascal
GPa	Giga Pascal
mg	Milligram
g	Gram
nm	Nanometer
μm	Micrometer
mm	Millimeter
cm	Centimeter
m	Meter
wt %	Weight percent
λ	Wave length
s	Second
min	Minutes
ε	Permittivity
tan δ	Tangent lost or dissipation factor
R _e	Electrodes resistance
R _g	Grain resistance
R _{gb}	Grain boundaries resistance

R_d	Domain resistance
C_g	Grain capacitances
C_{gb}	Grain boundaries capacitances
C_e	Electrodes capacitances

KESAN PENAMBAHAN LANTANUM OKSIDA (La_2O_3) KE ATAS

SIFAT-SIFAT KALSIUM KUPRUM TITANAT ($\text{CaCu}_3\text{Ti}_4\text{O}_{12}$)

ABSTRAK

Bahan elektroseramik $\text{CaCu}_3\text{Ti}_4\text{O}_{12}$ (CCTO) telah dihasilkan menggunakan kaedah tindak balas keadaan pepejal dengan menggunakan 3 jenis bahan mentah iaitu $\text{Ca}(\text{OH})_2$, CuO dan TiO_2 . Kajian ini merangkumi semua aspek pencirian bagi sifat-sifat CCTO yang disediakan dengan menggunakan kaedah lazim iaitu pengkalsinan dan pensinteran menggunakan relau pembakaran dan rawatan haba menggunakan ketuhar gelombang mikro. Kaedah dop dengan La telah dilakukan terhadap CCTO dengan penggantian Ca sebanyak 1 sehingga 10 % molar. Bahan mentah tersebut telah dicampur basah, dikalsin, dibentuk dan akhirnya disinter mengikut aliran pemrosesan. Campuran dikalsin pada suhu $900\text{ }^\circ\text{C}$ selama 12 jam menggunakan relau bagi pembentukan sebatian CCTO. Seterusnya pelet disinter pada suhu $1000\text{ }^\circ\text{C}$ selama 10 jam menggunakan relau tanpa pengaliran gas dan tiub relau dengan pengaliran gas argon semasa proses penyejukan. Kemudian, sampel yang telah disinter menggunakan relau dirawat haba dengan kaedah gelombang mikro selama 30 dan 60 minit. Ketumpatan semakin meningkat manakala keliangan semakin menurun dengan peningkatan molar bahan dop. Ujian XRD membuktikan pembentukan fasa CCTO. Analisis SEM mendapati bahawa saiz butiran semakin mengecil dengan penambahan peratus mol bahan dop bagi sampel yang disinter tanpa pengaliran gas argon dan menggunakan gas argon. Pemalar dielektrik adalah tinggi (~ 18000) dan nilai lesapan dielektrik adalah lebih bagus (~ 0.3) bagi sampel yang disintesis menggunakan gas berbanding sampel yang disinter tanpa pengaliran gas dengan menggunakan aluminium sebagai bahan elektrod. Walaubagaimanapun, keputusan ujikaji menunjukkan peningkatan pada pemalar dielektrik apabila

menggunakan perak sebagai elektrod. Analisis impedan bagi semua proses menunjukkan pemalar dielektrik semakin meningkat apabila rintangan sempadan butiran semakin menurun. Selain itu, penggunaan elektrod yang berbeza sebagai bahan saduran tidak memberikan perubahan pada rintangan butiran dan sempadan butiran bagi analisis impedan. Proses rawatan haba menggunakan kaedah gelombang mikro adalah lebih efektif yang mana kaedah ini dapat menghasilkan morfologi dan sifat dielektrik yang lebih bagus berbanding sampel yang tidak dirawat haba.

**EFFECT OF LANTHANUM OXIDE (La₂O₃) ADDITION ON THE
PROPERTIES OF CALCIUM COPPER TITANATE (CaCu₃Ti₄O₁₂)**

ABSTRACT

The electroceramic of CaCu₃Ti₄O₁₂ (CCTO) was prepared by solid state reaction method using three main raw materials of Ca(OH)₂, CuO, and TiO₂ powders. This study was focused in characterization of CCTO properties which was calcined and sintered through conventional and microwave sintering techniques. La doping method was applied to CCTO with substitution of Ca from 1 to 10 mole %. The starting materials were wet mixed, calcined, formed by pressing, and finally were sintered according the processing flow. The mixed powder was calcined at temperature of 900 °C for 12 hours using furnace to form the CCTO compound. CCTO pellet were sintered at 1000 °C for 10 hours using furnace under ambient air and synthesized under argon environment using tube furnace. Then, the samples that have been sintered using furnace were post heated using microwave method for 30 and 60 minutes. Density improved while the porosity decrease at higher dopant concentration. XRD analysis proved the formation of CCTO phase. SEM images shows that grain size becomes smaller for increasing the mole percent of doped material for sample synthesized with and without gas. Dielectric constant show higher value (~ 18000) and dielectric loss give better result (~ 0.3) for samples synthesized under argon environment compared to samples sintered without gas using aluminum electrode. Besides, the experimental results show a significant enhancement in dielectric behavior when using silver electrode. The impedance analysis shows that, the improvement of the dielectric constant mainly results from the decrease in the insulating property of the grain boundary. Moreover, using different electrode as coating material observed that there is no different in

impedance response where the result of resistance in grain and grain boundary for both samples evaporated in different electrode were similar to each other. Microwave treatment process is found to be effective where this technique produce better morphology and dielectric properties if compared to untreated samples.

CHAPTER 1

INTRODUCTION

1.1 Ceramic Materials

Ceramic materials are inorganic compounds consisting of metallic and non-metallic elements. They are mainly categorized as oxides, nitrides and carbides (Callister, 2000). Ceramic materials are brittle, hard, strong in compression, weak in shearing/tension and generally can withstand very high temperatures such as temperatures that range from 1000 °C to 1600 °C (Lehman et al., 1999). Moreover, ceramic have been traditionally admired for their unique electrical, optical and magnetic properties which become most important in technologies including communication, energy conversion, storage, electronics and automation. Such materials are now classified under electroceramics as distinguished from other functional ceramics such as advanced structural ceramics (Moulson and Herbert, 2003).

The term electroceramics are used to explain ceramics materials that have been formulated for electrical, magnetic or optical properties. These properties can be modified or designed in order to produce device with certain level of the properties. Examples of electrical properties are resistivity, conductivity, dielectric constant, dielectric loss, dielectric strength and capacitance. Different materials have their own unique properties which are characterized by intrinsic or extrinsic factors.

The performance of electroceramic materials and devices depends on the complex interplay between processing, structure and device physics. Topic areas cover a wide spectrum with recent active areas including sensors and actuators, electronic packaging, solid state ionics, defect and grain boundary, non-volatile

ferroelectric memories, high T_c superconductors and integrated dielectrics. The development in various subclasses of electroceramics is parallel to new technologies (Setter and Waser, 2000).

Electroceramics materials that have high dielectric constant can be used for construction of ceramic capacitor. Capacitors are important elements in electrical and electronic circuits, performing various functions that include blocking, coupling and decoupling, AC-DC separation, filtering, power factor correction, and energy storage. Capacitor component is size dependence for its capacitive properties. The properties are reduced by the reduction of plate area. So, in this case, higher dielectric material is required to maintain or increase the capacitance when the miniaturizing process is applied to the devices.

Dielectric materials have high electrical resistance but support the electric field efficiently. Lowering the dielectric loss will increase the efficiency of dielectric materials. The term dielectric material is used to explain the material which is electrical insulator or in which an electric field can be sustained with a minimal dissipation of power (Kao, 2004). The ideal of dielectric material does not exhibit electrical conductivity when an electric field is applied. In practice, all dielectrics do have some conductivity, which generally increases with the increase in temperature and applied field. If the applied field is increased to some critical magnitude, the material abruptly becomes conductive, a large current flows (often accompanied by a visible spark), and local destruction occurs to an extent depending upon the amount of energy which the source supplies to the low conductivity path. This critical field depends on the geometry of the specimen, the shape and material of the electrodes, the nature of the medium surrounding the dielectric, the time variation of the applied field, and other factors (Bassiouni et al., 2003).

Research interpreted that $\text{CaCu}_3\text{Ti}_4\text{O}_{12}$ (CCTO) may be part of electroceramic material where this material exhibits a high dielectric constant value of ~ 12000 measured at 1 kHz in room temperature (Bender and Pan, 2004). However, unlike most undoped ferroelectrics or relaxors, its dielectric constant shows very little temperature dependence between room temperature and $200\text{ }^\circ\text{C}$. As a result, this material has sparked great interest because of its potential use in microelectronics applications (Homes et al., 2001). Furthermore, $\text{CaCu}_3\text{Ti}_4\text{O}_{12}$ also can be used as dielectric material between two plates of capacitor to double its performance because of giant dielectric constant. Saji and Choe (2009), have produced low thickness CCTO thin films which can further increase capacitor performance.

Another study also had proven that CCTO may be classified as new class of oxide perovskites where high dielectric properties are different from classic ferroelectrics or relaxors. Unlike ferroelectrics, which show a great enhancement in permittivity near its Curie point (which is typically associated with a change in crystal structure), the dielectric constant of CCTO has been measured to be relatively stable from 100 to 600 K (Bender and Pan, 2004). Below 100 K the dielectric constant drops off dramatically to around 100. Neutron powder diffraction detects no change in crystal structure in the measured temperature range of 35–1273 K or higher (Moussa and Kennedy, 2001).

1.2 Preparation of $\text{CaCu}_3\text{Ti}_4\text{O}_{12}$ (CCTO)

Researcher and scientists around the globe are working for the development of high purity phase CCTO with improved powder morphology, which will enhance dielectric constant with low loss. Solid state synthesis has been chosen for this study in order to produce CCTO powder with high quality. However, there are many

opinions from other researcher about the preparation of CCTO. According to Ni et al. (2007), stoichiometric amounts of CCTO powders can be produced by wet ball milling with zirconia media for 12 hours, followed by calcination at 950 °C for 2 hours. Sintered was done at various temperature from 1100 to 1150 °C for different durations.

Different with Mohamed et al. (2007b), the stoichiometric ratios of the reagents were mechanically ball milled for 1 hour and then calcined at 900 °C for 12 hours. This preparation was continued with sintering process at 1050 °C for 12 hours. Bender and Pan (2004) also prepared the ceramic CCTO using conventional solid state techniques where the mixture powders obtained by attrition milling or mortar. Then, calcination process was done at 960 °C for 8 hours. The sintering condition was considered to be 1100 °C for 3 hours. Changes in temperature and time for calcinations and sintering process are very important in order to enhanced density and improved electrical properties.

Therefore, in this study, the calcination temperature of 900 °C for 12 hours and sintering temperature of 1000 °C with soaking time of 10 hours had been applied for La-doped CCTO.

1.3 Problem Statement

Cubic CCTO exhibits an enormously large dielectric response as reported by Subramanian and co-workers (2000) which reaches its level as high as 12 000 at 1 kHz. However, the dielectric loss of CCTO is too high for commercial applications. Mu et al. (2008) reported that the typical value of dielectric loss for CCTO ceramics is about 0.1 at 1 kHz measured at room temperature. It is necessary to know the

origin of dielectric loss in CCTO to find an effective method to lower it as needed for microelectronic and microwave device applications.

According to Moulson and Herbert (2003), the dielectric loss is due to the rotation of the atoms in an alternating electric field. The rotation of a dipole in a material is like a small ball rotating in a viscous fluid. Under an external force which is produced by electric field, it tends to change from its original equilibrium state to a new equilibrium state. This process is generally referred to the relaxation process.

Many researchers have proposed a ways to reduce dielectric loss and one of the solutions is by doping CCTO with other elements (Capsoni et al., 2004) such as SiO₂-doped CCTO (Kim et al., 2007), Zn-doped CCTO (Hutagalung et al., 2009), Fe- and Nb-doped CCTO (Grubbs et al., 2005), Cr₂O₃-doped CCTO (Kwon et al., 2008), CaTiO₃ doped CCTO (Yan et al., 2006), ZrO₂ doped CCTO (Patterson et al., 2005). Other than that, Feng et al. (2006) have introduced higher concentration (0.2 mole) of lanthanum oxide (La₂O₃) as doping material synthesized under normal atmosphere at higher temperature. The result for dielectric constant and dielectric loss at low frequency measurement was about 3000 and 0.015, respectively. However, there is no reported result on dielectric properties of La-doped CCTO at higher frequency (1 MHz to 1 GHz) where many potential applications of CCTO, such as wireless communication devices, operate in a frequency range of a few hundred MHz to a few GHz. This means that knowledge of high frequency properties of CCTO is very important.

Therefore, this study was focused on preparations of La-doped CCTO under argon environment with lower concentration of doping material in order to improve its dielectric properties. Besides, high frequency dielectric measurement was performed as a complimentary to the low frequency investigation.

1.4 Research Objectives

The specific objectives of the present study are as follows:

- i. To synthesis undoped and La-doped CCTO from starting material of $\text{Ca}(\text{OH})_2$, CuO , TiO_2 and La_2O_3 .
- ii. To investigate the structures, morphology, electrical and dielectric properties of prepared samples.
- iii. To improve the dielectric properties (higher dielectric constant and lower dielectric loss) of CCTO under argon environment measured at higher frequency (1 MHz to 1 GHz).

1.5 Research Overview

The processing and characterization of undoped and La-doped CCTO were carried out in conventional processing under argon environment and ambient air. Initially, the raw materials were characterized to identify the morphology and phase present. Undoped CCTO was prepared using material of $\text{Ca}(\text{OH})_2$, CuO , and TiO_2 while La_2O_3 with 0.01, 0.02, 0.03, 0.05 and 0.10 mole fraction was added to produce La-doped CCTO. The raw materials were mixed via wet milling for 2 hour using zirconia ball as the milling medium. As reported, the wet ball milling is faster than dry milling in term to produce the homogenous samples with high dispersion and high mobility of particles and this technique is very important for small quantity of doping elements to disperse successfully (Moulson and Herbert, 2003).

Subsequently, these mixtures were oven dried overnight. Later, this was followed by the calcinations of the mixed powder in alumina crucible at 900 °C using Electrical Carbolite Furnace and High Temperature Tube Furnace for 12 hours with 5°C/min as heating rate to become a loose and brown ash powder. This

temperature and soaking time were chosen with reference to the previous study (Mohamed et al., 2007b). Hereafter the following procedure, the powder was ground and pressed using hydraulic pressing under 300 MPa pressure to form the pellets with diameter of 13 mm and 18 mm and a thickness of ≤ 3 mm.

Finally, the yellowish pellets were sintered under two conditions. First, pellets were sintered at 1000 °C for 10 hours using Electrical Furnace without gas and then the sintered pellets were treated using microwave with different time. Second condition, sintering process was done using High Temperature Tube Furnace at 1000 °C for 10 hours where argon gas was applied at cooling stage.

The crystalline structures of the prepared samples were analyzed using X-ray powder diffraction (XRD). The microstructures of the samples were examined by using a Scanning Electron Microscopy (SEM) and Energy Dispersive X-ray (EDX). In order to measure the electrical properties, the sintered pellets were polished to produce a flat uniform surface. Then the pellets were evaporated by silver and aluminium electrodes using thermal evaporator. The electrical properties were measured by a precision Impedance Analyzer and Autolab machine. The flow chart for the experimental work is given in Figure 1.1.

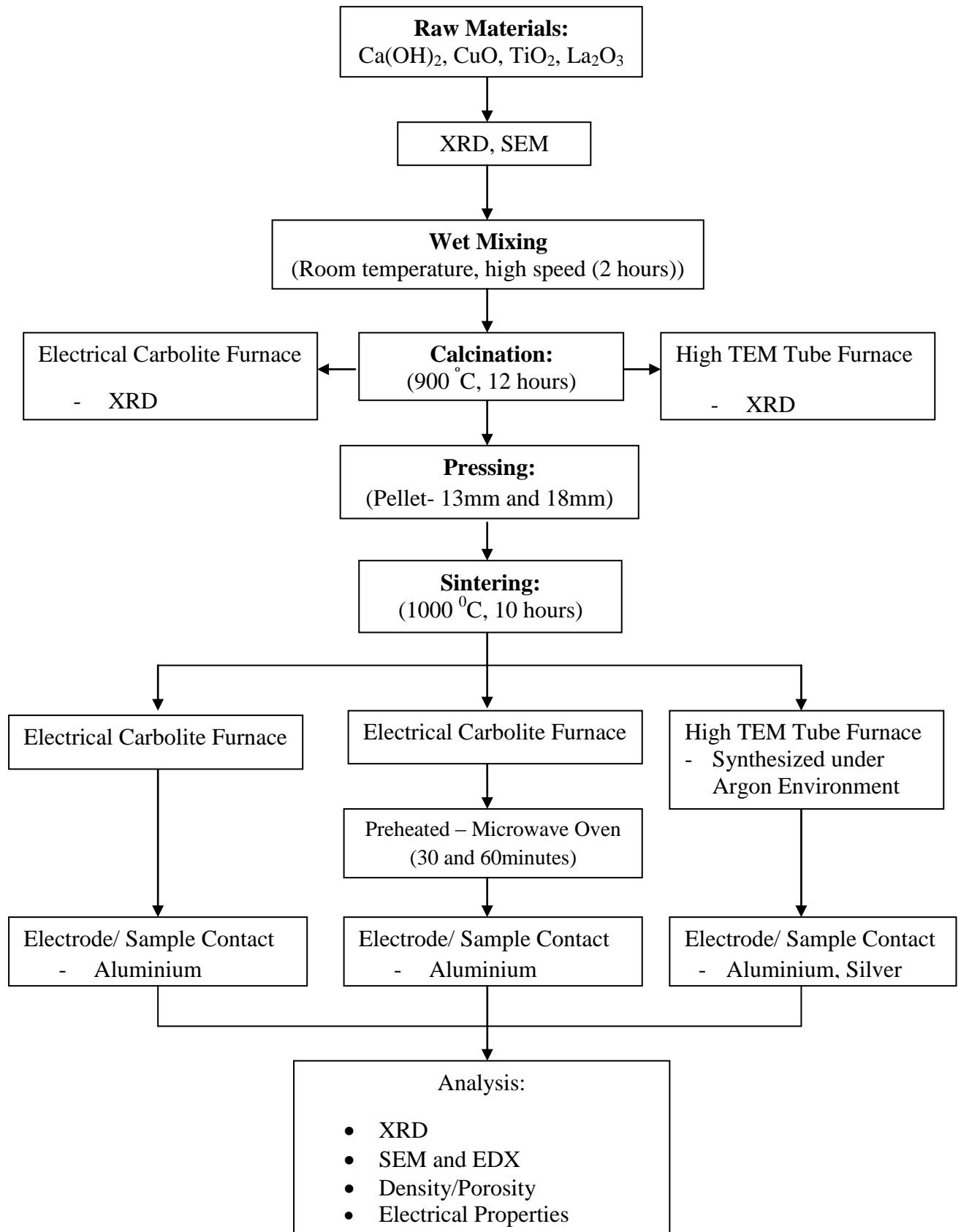


Figure 1.1: Process flow of experimental work.

CHAPTER 2

LITERATURE REVIEW

2.1 Introduction

Electroceramics is a class of ceramic materials that used primarily for their electrical, mechanical, thermal and chemical stability. These unique properties have become of increasing importance in many key technologies including communications, energy conversion and storage, electronics and automation. The various subclasses of electroceramics have paralleled the growth of new technologies including ferroelectrics (high dielectric capacitors), non-volatile memories, ferrites (data and information storage), solid electrolytes (energy storage and conversion), piezoelectric (sonar) and semiconducting oxides (environmental monitoring) (Moulson and Herbert, 1992). The grain boundaries, bulk material and surface effects are the main point for better result in dielectric constant, dielectric strength, electrical conductivity and power loss (Dutta and De, 2007).

2.2 Perovskite Structure

The general crystal structure which shown in Figure 2.1, is a primitive cube, with the A cation in the middle of the cube, the B cation in the corner and the anion, commonly oxygen, in the centre of the face edges. The structure is stabilized by the 6 coordination of the B cation (octahedron) and 12 of the A cation.

In 1839, Gustav Rose, a Russian mineralogist, discovered the perovskite structure in Ural mountain of Russia. This name perovskite has been later used for the designation of large perovskite family and was adopted by many oxides that have

the chemical formula ABO_3 . This versatile structure has many potential applications in ferroelectrics, catalysts, sensors and superconductors.

Generally, the most symmetry perovskite structure is in cubic form, with the presence of cation-A located at corner part cubic, cation-B located at body centre cubic while anion-O located at central face. This might be described as perovskite-related body centered cubic (bcc). The cations can be in various charges. Subramanian et al. (2003) cited that the space for A cation is essentially fixed, and the twelve equal A-O must be very close to 2.6 \AA for CCTO perovskite structure. Perovskite structure of ABO_3 is shown in Figure 2.1.

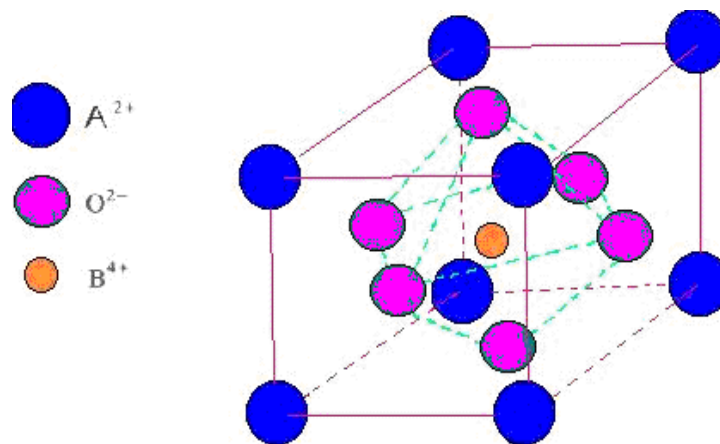


Figure 2.1: Perovskite simple cubic structures (Howard & Kennedy, 1999).

Elements of atom A usually in large size. The bigger size of cation A can cause structure size increment for overall AO_3 (bcc). Apart from that, this size also affect in minimum energy position of original octahedron that might be occupied by atom B. The exchange of atom caused by electric field and resulted electric dipole structure (Howard & Kennedy, 1999). Materials that have perovskite structure such as $MgTiO_3$, $PbTiO_3$, $CaTiO_3$, $BaTiO_3$ and also CCTO. Perovskites possess high values for dielectric and are widely used in such technological applications (Sanchez-Benitez et al., 2004).

2.3 CCTO

CCTO is a one of the compound that has perovskite structure. Homes et al. (2001) mentioned that CCTO have perovskite related body centered cubic (BCC). The combination structure of Ca^{2+} cation in the A site, Cu^{2+} cation in the B site while O_3 is occupied by oxygen is shown in Figure 2.2. The size difference between Ca^{2+} and Cu^{2+} causes the TiO_6 octahedra to undergo substantial tilting, leading to a body centred cubic supercell of space group $Im\bar{3}$ in which the Ti^{4+} ions occupy centrosymmetric position in the octahedral sites. The angle of tilt is sufficiently large that the Cu^{2+} ions occupy an essentially square-planer environment.

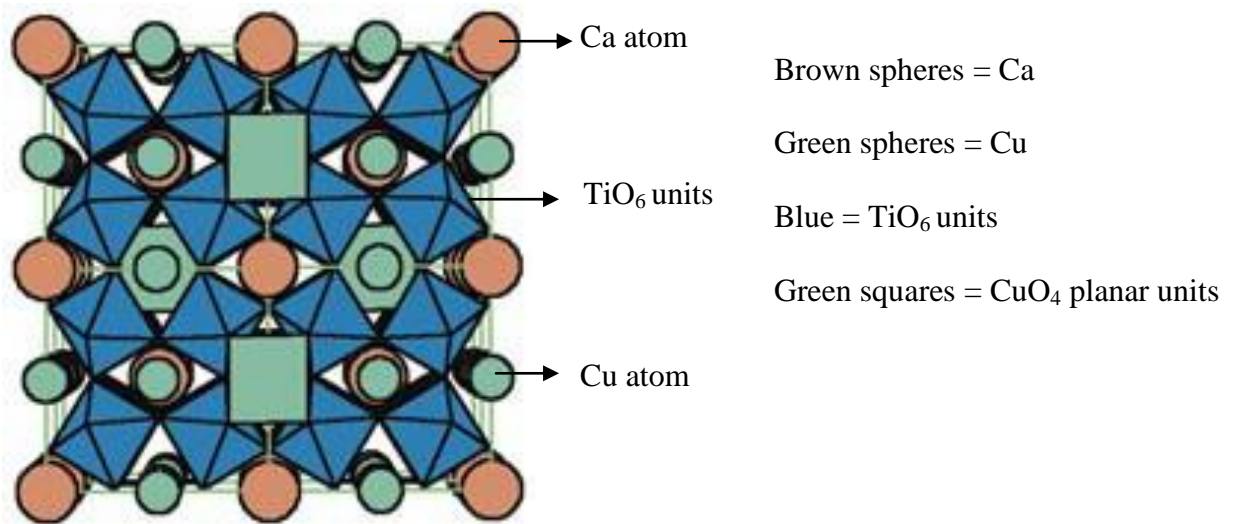


Figure 2.2: Crystal structure of CCTO (Homes et. al., 2001)

Recently, the dielectric properties of various $\text{ACu}_3\text{Ti}_4\text{O}_{12}$ and $\text{ACu}_3\text{Ti}_3\text{FeO}_{12}$ oxides (A = metal ions) were measured. Of the 13 oxides tested, CCTO showed exceptional properties. The room temperature dielectric constant of CCTO measured at 1 kHz was 12,000 (Bender & Pan, 2004). However, unlike most undoped ferroelectrics or relaxors its dielectric constant showed very little temperature

dependence between room temperature and 200 °C. As a result, this material has sparked great interest because of its potential use in microelectronics.

Research also indicates that CCTO may be part of a new class of oxide perovskites which high dielectric properties are different than classic ferroelectrics or relaxors. Unlike ferroelectrics, which show a great enhancement in permittivity near its Curie point (which is typically associated with a change in crystal structure), the dielectric constant of CCTO has been measured to be relatively stable from 100 to 600 K. Below 100 K the dielectric constant drops off dramatically to around 100 (Kobayashi & Terasaki, 2003). However, neutron powder diffraction detects no changes in crystal structure in the measured temperature range of 35–1273 K or higher.

Also investigated that improvement of electrical properties for CCTO ceramics is depending on grain boundary which plays an important role in the giant dielectric behaviour. In previous studies of CCTO, two classes of possible explanations for the giant dielectric response are intrinsic mechanism and extrinsic mechanism. Intrinsic mechanism means that the giant dielectric response is measured in a perfectly stoichiometric, defect-free and single-domain crystal of CCTO (Subramanian et al., 2000). Extrinsic mechanism means that the giant dielectric response is associated with defects, domain boundaries or other crystalline deficiencies (He et al., 2003).

Sinclair et al. (2002) reported that internal capacitive barrier layers of grain boundaries are responsible for the observed unusual dielectric response, instead of an intrinsic property of the crystal structure. The basic idea is that the grains are electrically semi-conductive and the grain boundaries are highly resistant, and the

conductivity of the entire sample is prevented by the presence of thin insulating blocking layers at the internal grain boundaries.

2.4 Dielectric Materials

Dielectric materials are insulators or poor conductor of electricity, but mostly an efficient supporter of electrostatic fields used for their exceptional dielectric properties. When a material is introduced between two plates of a metal, the total charge stored in the capacitor will be changed. The changed depends on the ability of the material to polarize under an electric field. The field may possibly cause a slight shift in the balance of charge within the material to form an electrical dipole (Callister, 2007).

2.4.1 Dielectric Properties

The dielectric constant is the ratio of the permittivity of a substance to the permittivity of free space. It is an expression of the extent to which a material concentrates electric flux, and is the electrical equivalent of relative magnetic permeability.

As the electric flux density increases, the dielectric constant increases, if all other factors remain unchanged. This enables objects of a given size, such as sets of metal plates, to hold their electric charge for long periods of time, and/or to hold large quantities of charge. Materials with high dielectric constants are useful in the manufacture of high-value capacitors (Brady and Clauser, 1991).

Capacitor is a passive electronic component that stores energy in the form of an electrostatic field. In its simplest form, a capacitor consists of two conducting plates separated by an insulating material called the dielectric. The capacitance is directly proportional to the surface areas of the plates, and is inversely proportional

to the separation between the plates (Kao, 2004). The capacitance, C is related to the quantity of charged stored on either plate, Q by

$$C = \frac{Q}{V} \quad (2.1)$$

where V is the voltage applied across the capacitor. The units of capacitance are Coulombs per volts, or Farads (F). If consider a parallel capacitor with a vacuum in the region between the plates as shown in Figure 2.3a, the capacitance can be computed from

$$C = \epsilon_0 \frac{A}{l} \quad (2.2)$$

where A represents the area of the plates and l is the distance between them. The parameter ϵ_0 , called the permittivity of a vacuum, is a universal constant having the value of 8.85×10^{-12} F/m (Hammami et al., 2008). If the dielectric materials is inserted into the region within the plates as shown in Figure 2.3b, then

$$C = \epsilon \frac{A}{l} \quad (2.3)$$

where ϵ is the permittivity of this dielectric medium, which will be greater in magnitude than ϵ_0 . The relative permittivity ϵ_r , often called the dielectric constant, is equal to the ratio

$$\epsilon_r = \frac{\epsilon}{\epsilon_0} \quad (2.4)$$

The value is greater than unity and represents the increase in charge storing capacity by insertion of the dielectric medium between the plates. The dielectric constant is one of the material properties, which must be considered for capacitor design (Callister, 2000).

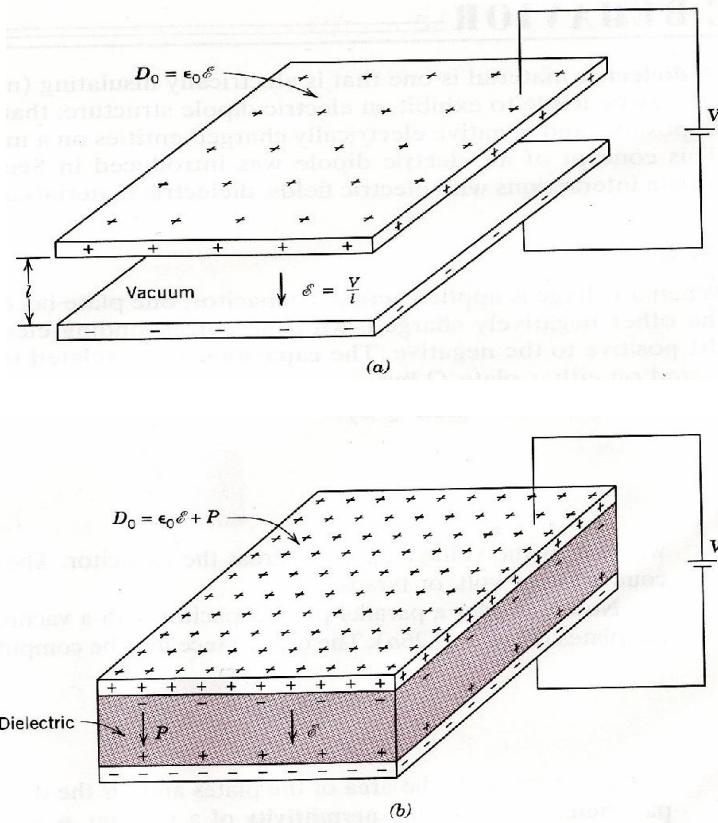


Figure 2.3: A parallel-plate capacitor (a) when a vacuum is present and (b) when a dielectric material is present (Callister, 2000).

The inserted dielectric material has increases the capacity by the factor of ϵ_r .

Table 2.1 lists the dielectric constant value for some dielectric materials at room temperature (Kahn et al., 1988).

Table 2.1: The value of dielectric constant for some materials at room temperatures (Kahn et al., 1988)

Material	Dielectric Constant
Teflon	2.1
Silica Glass	3.8
PVC	4.6
Al_2O_3	9.9
MgTiO_3	2
TiO_2	100
CaTiO_3	160
SrTiO_3	320
BaTiO_3	1000-2000

In dielectric materials, the loss tangent is a ratio of the loss permittivity to the real permittivity of a material (Kao, 2004). It is desirable to have a high dielectric constant and particularly a very small loss angle. Applications that are desirable to obtain a high capacitor in the smallest physical space, the high dielectric constant materials must be used and it is equally important to have a low value for the dissipation factor, $\tan \delta$ (Kingery et al., 1976).

2.4.2 Polarization Mechanisms

Dielectric constant mainly depends on the frequency of the alternating electric field or the rate of the change of the time varying field. Besides, it also depends on the chemical structure, imperfections or defects of the materials and other physical parameters including temperature or pressure. A dielectric material is made of atoms or molecules that possessed one or more basic types of electric polarization (Boch and Niepce, 2007).

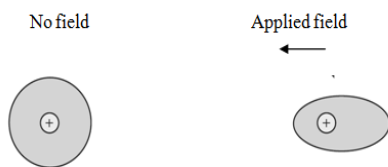
Polarization of the dielectric occurs when dielectric is placed in an electric field. There are four kinds of polarization mechanisms observed in ceramics as shown in Figure 2.4. In addition, ion jump polarization in glasses also exists in this mechanism. Electron polarization is one of the mechanisms where the shift of the centre of gravity of the negative electron cloud in relation to the positive atom nucleus in an electric field. Second mechanism is the displacement of positive and negative ions in relation to one another, which called ionic or atomic polarization. Third kind of polarization is associated with the presence of permanent electric dipoles which exist even in the absence of an electric field. A final source of polarization is mobile charges which are presence because they are impeded by

interfaces. The total polarizability of the dielectric, α can be represented as the sum of these mechanisms (Kingery et al., 1976)

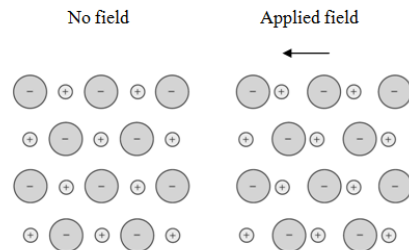
$$\alpha = \alpha_e + \alpha_i + \alpha_o + \alpha_s \quad (2.5)$$

where α_e is the electronic polarization, α_i is the ionic polarization, α_o is the orientation and α_s is the space charge.

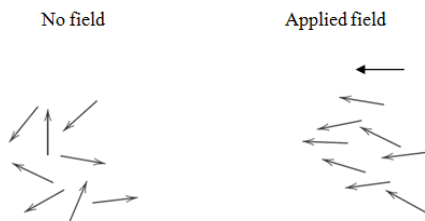
a) Electronic Polarization



b) Atomic Polarization



c) Orientation Polarization



d) Space Charge Polarization

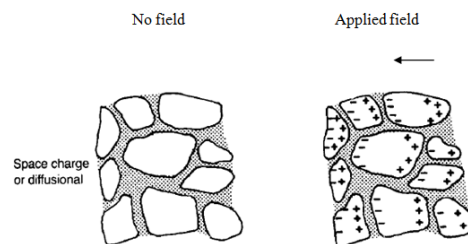


Figure 2.4: Schematic representation of different mechanisms of polarization (Wyatt and Hughes, 1974).

2.4.3 Impedance Spectroscopy

Impedance spectroscopy (IS) is a general term that subsumes the small signal measurement of the linear electrical response of a material of interest (including electrode effect) and the subsequent analysis of the response to yield useful

information about the physicochemical properties of the system. Other than that, IS usually applied to dielectric material which in solid or liquid non-conductors whose electrical characteristics involved dipolar rotation and to materials with predominantly electronic conduction (Macdonald, 1992).

Part from that IS also enables to separate the real and imaginary component of the complex electrical parameter in order to get true picture of material properties. Ranjan et al. (2009) investigated that IS technique was used to characterize microstructural and electrical properties of some electronic and ionic material based on analyzing the ac response of a system to a sinusoidal perturbation and subsequent calculation of impedance. Frequency dependent properties of a material can be interpreted from:

- i. complex impedance (Z^*), $Z^* = Z' - jZ''$
- ii. electric modulus (M^*), $M^* = 1/\varepsilon^*(\omega) = M' + jM''$
- iii. complex dielectric constant (ε^*)
- iv. tangent loss ($\tan \delta$), $\tan \delta = \varepsilon''/\varepsilon'$

where (Z' , M' , ε') and (Z'' , M'' , ε'') are the real and imaginary components of impedance, modulus and permittivity. The complex impedance of the ceramic configuration can be represented in terms of equivalent circuit representations by a series combination of RC elements (Macdonald, 1987).

2.4.3.1 Impedance Spectroscopy of CCTO

Impedance spectroscopy is a technique which initially used in electrochemical systems but nowadays, according to Beltran et al. (2003) this technique is famously used for characterizing electroceramics. The main thrust in

this approach is the assumption of an equivalent circuit to describe the electrical response of the sample. By varying the frequency of the applied sinusoidal electric field, measurement of the impedance can be made where data fitting can be employed to estimate the appropriate electrical circuit. Considering that current path has the same direction of the applied electric field, the equivalent circuit of the model is formed by the series combination of two parallel RC circuits, one representing the grain effect, R_g (low resistive component) and the other is the grain boundaries, R_{gb} (high resistive component) as shown in Figure 2.5. According to Prakash and Varma (2006) this presented model of equivalent circuit mostly appears at low frequency and can be found when measuring the Cole-Cole plots for undoped CCTO.

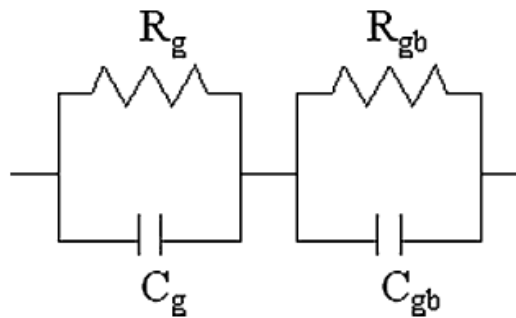


Figure 2.5: An equivalent circuit for electroceramic (Nobre and Lanfredi, 2003, Prakash and Varma, 2006)

Moreover, another simplest equivalent circuit which is a series of networks of three parallel RC elements, that has been applied successfully in the CCTO ceramics shown in Figure 2.6. Each element represents one of the responses of grain; grain boundary and electrode interface (Liang et al., 2006). This model is usually can be observed at higher frequency and using dopant material for CCTO preparation.

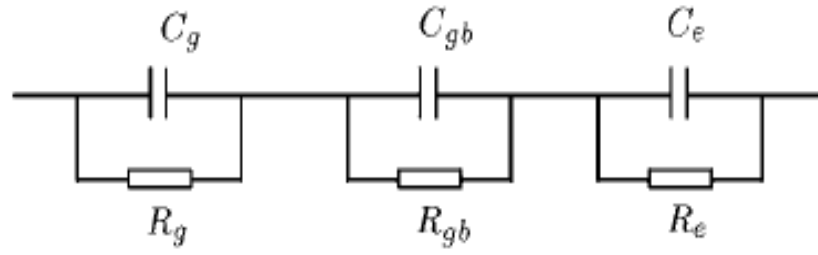


Figure 2.6: The RC equivalent circuit model, R_g , C_g ; R_{gb} , C_{gb} ; and R_e , C_e are the resistance and capacitances associated with grain, grain boundaries and the electrodes (Liang et al., 2006).

In addition, IS provides the information about the resistivity of the sample. The real axis intercepts of the complex impedance plane plots give values for the resistance of the grain boundary and bulk components. According to the previous study, the grain boundaries capacitances of ceramic CCTO were greater than the grain capacitance of the bulk component. This phenomenon happen because of the much smaller thickness compared to the grain volume. By assuming the $C_{gb} \gg C_b$ and $R_{gb} \gg R_b$, the capacitance of the sample may be approximated by Equations 2.6 and 2.7

$$C^* = C_b - j \frac{1}{\omega R_b} \quad \text{when } \omega \gg \frac{1}{C_{gb}R_b} \quad (2.6)$$

$$C^* = C_{gb} - j \frac{1}{\omega R_{gb}} \quad \text{when } \omega \ll \frac{1}{C_{gb}R_b} \quad (2.7)$$

This equation means, when the bulk and grain boundaries components are very dissimilar in magnitude, the capacitance at a fixed frequency far from a relaxation frequency is dominated by either of two components. Li et al. (2005) noted that the larger resistivity of grain boundary compared to the bulk component commonly cause the resistivity measurements to be dominated by the grain boundary

component. Moreover, the grain boundary capacitance remains uncharged with temperature, means R_b should decrease because of its semiconducting properties. Therefore, the relaxation time ($\tau = R_b C_{gb}$) should increase with increasing temperature. The activation energies measured by these authors were lower than elsewhere which explain that lower activation energies of ceramic CCTO is being due to the oxygen vacancies introduced after sintering at high temperature.

Other researchers considered that dielectric properties of CCTO were influenced by microstructure. Assuming that the equivalent circuit for CCTO be made up of two parallel R elements to represent the grain bulk and grain boundary element, the effective dielectric constant that can be expressed by Equation 2.8

$$\varepsilon = (R_b^2 C_b + R_{gb}^2 C_{gb}) / (C_0 (R_b + R_{gb})^2) \quad (2.8)$$

where subscript b and gb represent the grain bulk and grain boundary contributions, while C_0 is the capacitance of an equivalent cell volume in vacuum. Since $R_{gb} \gg R_b$ and $C_{gb} \gg C_b$, the effective dielectric constant is almost dependent on the grain boundary contribution,

$$\varepsilon \approx (C_{gb}) / (C_0) \quad (2.9)$$

When using the brick layer model, the author assumed that element to be made up of a layer grain boundary and a layer of grain bulk. If the grain bulk is negligible, the effective dielectric constant may be expressed by

$$\varepsilon \approx \varepsilon_{gb} ((d_{gb} + d_b) / (d_{gb})) \quad (2.10)$$

Therefore, the total dielectric constant was influenced greatly by thickness of grain boundary which in small size or the grain becomes large. So, based on previous study by Prakash and Varma (2006) the reason for the abnormally high dielectric

constant in ceramic CCTO is due to the ease at which the Cu segregates to the grain boundaries to form an internal barrier layer capacitance mechanism.

Sundaram (1994) has suggested that complex plane impedance analysis also can be used to investigate the effect of electrode on semiconducting ceramics. Based on his study, the semicircular arc appeared at similar high frequency ranges for all electrodes (In, In-Ga and Ag). However, when Ni electrode was used during measurement, the result only showed a real axis intercept. This scenario happens because there is no dielectric relaxation leading to the appearance of a semicircular arc which occurred in the sample. Moreover, above 10 MHz or below 10 kHz, no data can be collected.

Another study done by Basu and Maiti (1986) was observed a semicircle corresponding to the specimen-electrode interface in an electrodeless-Ni-deposited semiconducting BaTiO₃. Investigation revealed that this anomalous behaviour may be attributed to the shorting out of the interfacial impedance. A proposed equivalent circuit of electrode effect on ceramic materials is shown in Figure 2.7. Previous research also considered that by using this circuit, different resistive and capacitive elements can be observed.

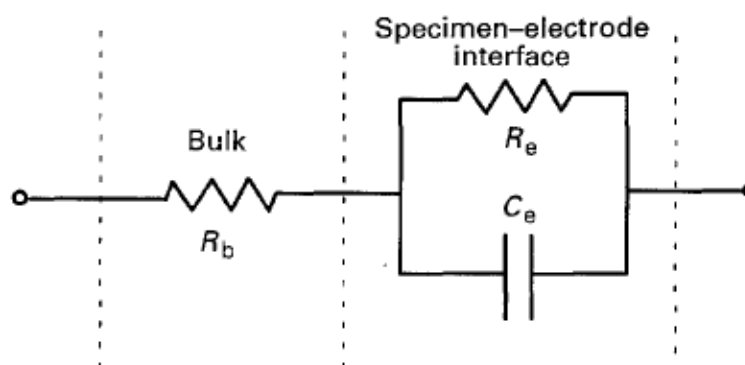


Figure 2.7: Equivalent circuit of electrode effect on ceramic material (Sundaram, 1994).

2.5 Grains Boundaries Effect

Grain boundaries play a major role in the dielectric properties of CCTO (Zang et al., 2005). When an impedance spectroscopy analysis done on $\text{CaCu}_3\text{Ti}_4\text{O}_{12}$ ceramics, the data shown that they are electrically heterogeneous and consist of semiconducting grains with insulating grain boundaries. Sinclair et al. (2002) suggested that the giant dielectric response is due to a grain boundary (internal) barrier layer capacitance (IBLC).

According to the report of Martirena and Burfoot (1974), the highest value of the permittivity is observed at a grain size of 1-0.7 μm . Figure 2.8 also shows that when grain size is smaller than critical size (about 1 μm), the energy of the domain wall can cancel the energy of elastic strain from lattice distortion. The energy of grain boundaries is direct proportional to the square of the grain diameter, and the strain energy is also directly proportional to the square of grain diameter. It is argued that the internal stress among grains affects the dielectric constant.

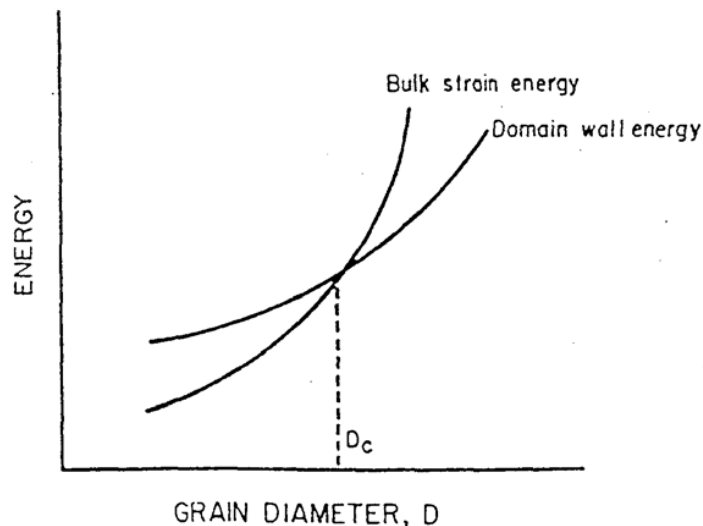


Figure 2.8: Limiting grain size for ferroelectric domain formation (Goodman et al., 1991)

Investigation by Ni et al. (2006) using Scanning Electron Microscope (SEM) done on the CCTO ceramic samples, found that sample sintered at 1125 °C/3 hours seems to be denser and exhibits a larger dielectric constant in comparison with the sample sintered at 1025 °C for 3 hours. However, a small percentage of Cu₂O secondary phase were detected in the samples sintered at 1125 °C. More secondary phases with Cu-rich composition were observed when increasing the sintering temperature above 1075 °C. Moreover, the variation of lattice constant also decreased with increasing the sintering temperature.

Ni et al. (2006) also investigated on dielectric properties of CCTO ceramics where the value for dielectric constant at 10 kHz increases from 3790 to 53,120 with increasing the sintering temperature from 1025 to 1125 °C. The room temperature dielectric constant of 53,120 at 10 kHz is much higher than most of that reported previously (Ramirez et al., 2000), and prove the result for the long time sintered situation (Adams et al., 2002). In addition, the dielectric constant for the samples sintered at 1100 °C is slightly lower than samples sintered at 1075 °C and this happen due to the poor network structure of secondary phases, which might be concerning with the transforming from CuO to Cu₂O.

Another studied done by Prakash and Varma (2006) found that different time of sintering with same temperature also led to change in dielectric behaviour. Result indicated that the dielectric constant for the sample sintered at 1100 °C for 2.5 hour is only 2400 at 10 kHz. Nevertheless, when the sintering duration was increased to 5 hours, the dielectric constant improved to 13,000 at 10 kHz. They described that this situation happened because of the remarkable change in the microstructure in which some grains show abnormal growth and Cu-rich smaller grains occupying the

intermittent regions. Further increase in the sintering duration up to 15 hour increased the dielectric constant to more than 24,000.

2.6 Processing effect

The effect of processing plays a major role especially for improving the dielectric constant of CCTO. Many researchers reported that dielectric constant of CCTO was highly dependent on the processing conditions such as milling time, sintering temperature, duration of sintering, etc. (Zang et al., 2005). The dielectric constant ranging from 2000 to 80,000 was achieved by varying the sintering temperature and ascribed to giant barrier layer effects at the grain boundary.

Besides, different preparations of the sample also give influence to the value for the electrical properties. According to Bender and Pan (2004), CCTO powders was prepared via mortar and pestle, known as conventional ceramic solid state reaction processing techniques and the value of room temperature permittivity was 11,700 with 0.047 dielectric losses. However, when using attrition mill, the permittivity value was close to 100,000. Sintering temperature for CCTO also effect the dielectric constant value. Increasing the sintering temperature from 990 to 1050 °C, dielectric constant gives higher value (714 to 82,450) and reduces the dielectric loss of the ceramics sample (0.014 to 0.98). Moreover, Bender and Pan (2004) found that annealing their sample in argon at 1000 °C drastically increased the dielectric constant close to 1,000,000 with a corresponding increase in the loss. They attributed this to an increase in the oxygen vacancies and subsequently available the charge carriers.

Duration of sintering is very essential in determining the value of dielectric constant. The value for dielectric constant was found to increase with the soaking